symmetry

Article

Impact of Nonlinear Thermal Radiation and the Viscous Dissipation Effect on the Unsteady Three-Dimensional Rotating Flow of Single-Wall Carbon Nanotubes with Aqueous Suspensions

Muhammad Jawad [1], Zahir Shah [1], Saeed Islam [1], Jihen Majdoubi [2], I. Tlili [3], Waris Khan [4] and Ilyas Khan [5,*]

1 Department of Mathematics, Abdul Wali Khan University, Mardan, Khyber Pakhtunkhwa 23200, Pakistan; muhammadjawad175@yahoo.com (M.J.); zahir1987@yahoo.com (Z.S.); saeedislam@awkum.edu.pk (S.I.)
2 Department of Computer Science, College of Science and Humanities at Alghat Majmaah University, Al-Majmaah 11952, Saudi Arabia; j.majdoubi@mu.edu.sa
3 Department of Mechanical and Industrial Engineering, College of Engineering, Majmaah University, Al-Majmaah 11952, Saudi Arabia; l.tlili@mu.edu.sa
4 Department of Mathematics, Kohat University of Science and technology, Kohat, KP 26000, Pakistan; Wariskhan758@yahoo.com
5 Faculty of Mathematics and Statistics, Ton Duc Thang University, Ho Chi Minh City 72915, Vietnam
* Correspondence: ilyaskhan@tdt.edu.vn

Received: 30 December 2018; Accepted: 31 January 2019; Published: 12 February 2019

Abstract: The aim of this article is to study time dependent rotating single-wall electrically conducting carbon nanotubes with aqueous suspensions under the influence of nonlinear thermal radiation in a permeable medium. The impact of viscous dissipation is taken into account. The basic governing equations, which are in the form of partial differential equations (PDEs), are transformed to a set of ordinary differential equations (ODEs) suitable for transformations. The homotopy analysis method (HAM) is applied for the solution. The effect of numerous parameters on the temperature and velocity fields is explanation by graphs. Furthermore, the action of significant parameters on the mass transportation and the rates of fiction factor are determined and discussed by plots in detail. The boundary layer thickness was reduced by a greater rotation rate parameter in our established simulations. Moreover, velocity and temperature profiles decreased with increases of the unsteadiness parameter. The action of radiation phenomena acts as a source of energy to the fluid system. For a greater rotation parameter value, the thickness of the thermal boundary layer decreases. The unsteadiness parameter rises with velocity and the temperature profile decreases. Higher value of ϕ augments the strength of frictional force within a liquid motion. For greater R and θw; the heat transfer rate rises. Temperature profile reduces by rising values of Pr.

Keywords: unsteady rotating flow; porous medium; aqueous suspensions of CNT's; nonlinear thermal radiation; viscous dissipation effect; HAM

1. Introduction

The recent period of technology and science has been totally affected by nanofluids, and they possess an important role in various engineering and machinery uses, like biomedical applications, detergency, transferences, industrialized cooling, microchip technology and nuclear reactions. By adding nanoparticles, mathematicians and physicists developed to a way to increase the capacity of heat transfer in the base fluid. The investigators applied advanced techniques, like in the base fluids, by adding ultra-fine solid particles. Heat transfer and single-phase higher thermal conductivity coefficients are greater in nanofluids as compared to bottom liquids. Khan [1] has examined Buongiorno's model with heat transfer and mass for nanofluid flow. Mahdy et al. [2] have applied Buongiorno's model for nanofluid flow with heat transfer through an unsteady contracting cylinder. Malvandi et al. [3] have described flow through a vertical annular pipe. In [4–6], researchers have examined the flow of nanofluids through a stretching sheet. Ellahi [7] has discussed nanofluid flow through a pipe with the MHD effect. Nanofluid flow through a cone has been deliberated by Nadeem et al. [8]. Abolbashari et al. [9] have debated entropy generation for the analytical modelling of Casson nanofluid flow. A mixture of suspended metallic nanoscale particles with a base fluid is known as a mixture of nanoparticles, the word nanofluid was invented by Choi [10]. Nanofluids were formulated for heat transport, momentum and mass transfer by Buongiorno, in order to obtain four equations of two components for non-homogeneous equilibrium models [11]. Most of the research available on the nanofluid problem is cited in works [12–14]. Presently, in these studies, few significant attempts have been presented for nonlinear thermal radiation [15]. Kumar et al. [15] have reported the rotating nanofluid flow problem with deliberation of dissimilar types of nanoparticles, including entropy generation to use the second law of thermodynamics. Nadeem et al. [16] have studied the inclusion of nanoparticles of titanium and copper oxide, which related to the rotating fluid flow problem. Mabood et al. [17] have studied the flow of rotating nanofluid and the impact of magnetic and heat transfer. Shah et al. [18,19] have deliberated a rotating system nanofluid flow with hall current and thermal radiation. Gireesha et al. [20] have examined a single-wall nanotube in an unsteady rotating flow with heat transfer and nonlinear thermal radiation. Currently, Ishaq et al. [21] have discussed the thermal radiation effect with respect to the entropy generation of unsteady nanofluid thin film flow on a porous stretching sheet. In the field of nanoscience, the study of the flow of fluid with nanoparticles (nanofluids) holds a great amount of attention. Nanofluids scattered with 10^9 nm sized materials are arranged in fluids such as nanofibers, droplets, nanoparticles, nanotubes etc. Solid phase and liquid phase are the two period systems. To augment the thermal conductivity of fluids, nanofluids can be applied, and they thrive in stable fluids, exhibiting good writing and dispersion properties on hard materials [22,23]. Sheikholeslami et al. [24–26] have described the significance of nanofluids in in nanotechnology. Yadav et al. [27–29] have deliberated nanofluids with the MHD effect by using dissimilar phenomena, further study of heat transfer enhancement, numerical simulation, stability and instability with linear and non-linear flows of nanofluid. The Darcy–Forchheimer flow of radiative carbon nanotubes (CNTs) in nanofluid in a rotating frame has been investigated by Shah et al. [30–33]. Dawar et al. [33] have studied CNTs, Casson MHD and nanofluid with radiative heat transfer in rotating channels. Khan et al. [34] have studied three-dimensional Williamson nanofluid flow over a linear stretching surface. Shah et al. [35] have described the analysis of a micropolar nanofluid flow with radiative heat and mass transfer. Khan et al. [36,37] have discussed the Darcy–Forchheimer flow of micropolar nanofluid between two plates. Shah et al. [38] have described MHD thin film flow of Williamson fluid over an unsteady permeable stretching surface. Jawad et al. [39] have investigated the Darcy–Forchheimer flow of MHD nanofluid thin film flow with Joule dissipation and Navier's partial slip. Khan et al. [40] have investigated the slip flow of Eyring–Powell nanoliquid. Hammed et al. [41] have described a combined magnetohydrodynamic and electric field effect on an unsteady Maxwell nanofluid flow. Dawar et al. [42] have described unsteady squeezing flow of MHD CNT nanofluid in rotating channels. Khan et al. [43] have investigated the Darcy–Forchheimer flow of MHD CNT nanofluid with radiative thermal aspects. Sheikholeslami et al. [44] have investigated the uniform magnetic force impact on water based nanofluid with thermal aspects in a porous enclosure. Feroz et al. [45] have examined the entropy generation of carbon nanotube flow in a rotating channel. Alharbi et al. [46] have described entropy generation in MHD Eyring–Powell fluid flow over an unsteady oscillatory porous stretching surface with thermal radiation. Liao [47] learned in 1992 that this method was a fast way to find the approximate solution and that for the solution of nonlinear problems it was a better fit.

The main objective of this article is to investigate the augmentation of heat transfer in time dependent rotating single-wall carbon nanotubes with aqueous suspensions under the influence of nonlinear thermal radiation in a permeable medium. The impact of viscous dissipation is taken into account. For the solution, the homotopy analysis method (HAM) [48–50] is applied. The effect of numerous parameters on the temperature and velocity fields are explained by graphs.

2. Problem Formulation

We considered a three-dimensional time dependent electrically conducting incompressible laminar rotating flow of nanofluid. Aqueous suspensions of single-wall CNTs based on water were assumed as a nanoscale materials with a porous medium. The x, y and z variables are the Cartesian coordinates where $\Omega(t)$ is angular velocity of the rotating fluid, which is measured about the z-axis. The surface velocities in the x and y axes are taken as $u_w(x,t) = \frac{bx}{(1-\delta t)}$ and $v_w\,(x,\ t)$ respectively, and $w_w(x,t)$ is the velocity in the z-axis, known as the mass flux wall velocity. The governing equations under these assumptions are taken in the form as [4,14,18]

$$\frac{\partial u}{\partial x} + \frac{\partial v}{\partial y} + \frac{\partial w}{\partial z} = 0 \tag{1}$$

$$\frac{\partial u}{\partial t} + u\frac{\partial u}{\partial x} + v\frac{\partial u}{\partial y} + w\frac{\partial u}{\partial z} + \frac{2\Omega v}{1-\delta t} = -\frac{1}{\rho}\frac{\partial P}{\partial x} + \frac{\mu_{nf}}{\rho_{nf}}\frac{\partial^2 u}{\partial z^2} - \frac{\sigma\beta_0^2}{1-\delta t}u - \frac{\mu_{nf}}{k^*}\frac{u}{1-\delta t} \tag{2}$$

$$\frac{\partial v}{\partial t} + u\frac{\partial v}{\partial x} + v\frac{\partial v}{\partial y} + w\frac{\partial v}{\partial z} + \frac{2\Omega u}{1-\delta t} = -\frac{1}{\rho}\frac{\partial P}{\partial y} + \frac{\mu_{nf}}{\rho_{nf}}\frac{\partial^2 v}{\partial z^2} - \frac{\sigma\beta_0^2}{1-\delta t}v - \frac{\mu_{nf}}{k^*}\frac{v}{1-\delta t} \tag{3}$$

$$\frac{\partial w}{\partial t} + u\frac{\partial w}{\partial x} + v\frac{\partial w}{\partial y} + w\frac{\partial w}{\partial z} = -\frac{1}{\rho}\frac{\partial P}{\partial z} + \frac{\mu_{nf}}{\rho_{nf}}\frac{\partial^2 w}{\partial z^2} \tag{4}$$

$$\frac{\partial T}{\partial t} + u\frac{\partial T}{\partial x} + v\frac{\partial T}{\partial y} + w\frac{\partial T}{\partial z} = \alpha_{nf}\frac{\partial^2 T}{\partial z^2} + \frac{1}{(\rho c_p)_{nf}}\frac{\partial q_r}{\partial z} + \frac{\mu_{nf}}{(\rho c_p)_{nf}}\left[\left(\frac{\partial u}{\partial z}\right)^2 + \left(\frac{\partial v}{\partial z}\right)^2\right] \tag{5}$$

The corresponding boundary conditions are given as

$$\begin{array}{ll} u = u_w(x,t), v = 0, w = 0, T = T_w & at \quad z = 0 \\ u \to 0, v \to 0, w \to 0, T \to T_\infty & at \quad z \to \infty. \end{array} \tag{6}$$

where x, y and z, are the directions of the velocity components. The angular velocity of the nanofluid is denoted as Ω, nanofluid dynamic viscosity is denoted as μ_{nf}, the nanofluid density is denoted as ρ_{nf}, the nanofluid thermal diffusivity is denoted as α_{nf}, temperature of the nanofluid is denoted as T, T_w and T_∞ denotes the wall and outside surface temperature, respectively.

The expression of radiative heat flux in Equation (5) is written as:

$$q_r = -\frac{4\sigma^*}{3(\rho c_p)_{nf}k^*}\frac{\partial T^4}{\partial z} = -\frac{16\sigma^*}{3k^*}T^3\frac{\partial T}{\partial z} \tag{7}$$

where the mean absorption coefficient is denoted by k^* and the Stefan–Boltzman constant is denoted by σ^*. By using Equation (7) in Equation (5), this produces the following equation:

$$\begin{array}{l} \frac{\partial T}{\partial t} + u\frac{\partial T}{\partial x} + v\frac{\partial T}{\partial y} + w\frac{\partial T}{\partial z} \\ = \alpha_{nf}\frac{\partial^2 T}{\partial z^2} + \frac{16\sigma^*}{(\rho c_p)_{nf}k^*}\left[T^3\frac{\partial^2 T}{\partial z^2} + 3T^2\left(\frac{\partial T}{\partial z}\right)^2\right] + \frac{\mu_{nf}}{(\rho c_p)_{nf}}\left[\left(\frac{\partial u}{\partial z}\right)^2 + \left(\frac{\partial v}{\partial z}\right)^2\right] \end{array} \tag{8}$$

α_{nf},μ_{nf} and ρ_{nf} are interrelated with ϕ, which is denoted as:

$$\begin{aligned} &\rho_{nf} = \left(1-\phi+\phi\left(\tfrac{(\rho_s)_{CNT}}{\rho_f}\right)\right), \mu_{nf} = \tfrac{\mu_f}{(1-\phi)^{2.5}}, \alpha_{nf} \\ &= (1-\phi)\left(\rho_f\right)_f + \phi(\rho_s)_{CNT}, \\ &\left(\rho C_p\right)_{nf} = (1-\phi)\left(\rho C_p\right)_f + \phi\left(\rho C_p\right)_{CNT}, \tfrac{k_{nf}}{k_f} \\ &= \frac{1-\phi+2\phi\left(\frac{k_{CNT}}{k_{CNT}-k_f}\right)\ln\left(\frac{k_{CNT}+k_f}{2k_f}\right)}{1-\phi+2\phi\left(\frac{k_f}{k_{CNT}-k_f}\right)\ln\left(\frac{k_{CNT}+k_f}{2k_f}\right)} \end{aligned} \tag{9}$$

The volumetric heat capacity of the CNT and base fluid is denoted by $\left(\rho C_p\right)_{CNT}$ and $\left(\rho C_p\right)_f$ respectively. Nanofluid thermal conductivity is denoted as k_{nf}, base fluid thermal conductivity is denoted by k_f, CNT thermal conductivity is denoted by k_{CNT}, nanoparticle volume fraction is denoted by ϕ, the base fluid density viscosity is denoted by ρ_f and CNT density is denoted by ρ_{CNT}.

Similarity transformations are now introduce as:

$$\begin{aligned} &u = \tfrac{bx}{(1-\delta t)} f'(\eta),\ v = \tfrac{bx}{(1-\delta t)} g(\eta), w = -\sqrt{\tfrac{b\nu}{(1-\alpha t)}} f(\eta),\ \eta = \sqrt{\tfrac{b}{\nu(1-\alpha t)}} z \\ &\mathrm{T} = \mathrm{T}_\infty(1+(1-\delta t)\theta(\eta)) \end{aligned} \tag{10}$$

Inserting Equation (10) in Equations (2)–(6), we have:

$$\begin{aligned} &\frac{1}{(1-\phi)^{2.5}\left((1-\phi)+\phi\frac{(\rho_s)_{CNT}}{\rho_f}\right)} f^{iv} - \frac{\beta_0^2}{\lambda} f'' - \frac{\mu_{nf}}{(1-\phi)^{2.5} k^* b} f'' \\ &-\left[\lambda\left(f' + \tfrac{\eta}{2} f''\right) + f'f'' - ff'' - 2\tfrac{\Omega}{b} g'\right] = 0 \end{aligned} \tag{11}$$

$$\begin{aligned} &\frac{1}{(1-\phi)^{2.5}\left((1-\phi)+\phi\frac{(\rho_s)_{CNT}}{\rho_f}\right)} g''' - \frac{\beta_0^2}{\lambda} g' + \frac{\mu_{nf}}{(1-\phi)^{2.5} k^* b} g' \\ &-\left[\lambda\left(g' + \tfrac{\eta}{2} g''\right) + gf'' - fg'' - 2\tfrac{\Omega}{b} f''\right] = 0 \end{aligned} \tag{12}$$

$$\begin{aligned} &\theta'' + R\left[(1+(\theta_w-1)\theta)^3\theta'' + 3(1+(\theta_w-1)\theta)^2(\theta_w-1)\theta'^2\right] + \tfrac{Ec}{\mathrm{Pr}}\left(f''^2 + g'^2\right) \\ &-\tfrac{1}{\mathrm{Pr}}\left[\lambda\tfrac{\eta}{2}\theta' - f\theta'\right] = o \end{aligned} \tag{13}$$

The boundary conditions are written as:

$$\begin{aligned} &f(0) = 0, f'(0) = 1, g(0) = 0, \theta(0) = 1, \quad at \quad \eta = 0 \\ &f'(\eta) \to 0, g(\eta) \to 0, f(\eta) \to 0, \theta(\eta) \to 0. \quad at \quad \eta \to \infty. \end{aligned} \tag{14}$$

Here, Ω denotes the rotation parameter and is defined as $\Omega = \frac{\omega}{b}$, and λ represents the unsteadiness parameter, defined as $\lambda = \frac{\delta}{b}$. R is radiation parameter, defined as $R = \frac{16\sigma^* \mathrm{T}_\infty^3}{3k_{nf}k^*}$. Pr is Prandtl number, defined as $\mathrm{Pr} = \frac{\alpha_{nf}}{\nu_{nf}}$. Ec represents the Eckert number, defined as $\mathrm{Ec} = \frac{u_w^2}{c_p(\mathrm{T}-\mathrm{T}_\infty)}$. The temperature ratio parameter is denoted by θ_w and $\theta_w = \frac{\mathrm{T}_w}{\mathrm{T}_\alpha}$.

Physical Quantities of Interest

In the given problem, the physical quantities of interest are C_{fx}, C_{fy} and Nu_x, which is denoted as:

$$C_{fx}\frac{\tau_{wx}}{\rho_f \mathrm{u}_w^2(x,t)}, C_{fy}\frac{\tau_{wy}}{\rho_f \mathrm{u}_w^2(x,t)}, Nu_x = \frac{xq_w}{(T_w - T_\infty)} \tag{15}$$

The surface heat flux is denoted by q_w, and τ_{wx} and τ_{wy} are surface shear stress, which are written as:

$$\tau_{wx} = \mu_{nf}\left(\frac{\partial u}{\partial z}\right)_{z=0}, \tau_{wy} = \mu_{nf}\left(\frac{\partial v}{\partial z}\right)_{z=0} \, and \, q_w = -k_{nf}\left(\frac{\partial T}{\partial z}\right) + (q_r)_{z=0}. \tag{16}$$

By the use of Equations (15) and (16), then we have:

$$\sqrt{\mathrm{Re}_x}C_{fx} = \frac{1}{(1-\phi)^{2.5}}f''(0), \sqrt{\mathrm{Re}_x}C_{fy} = \frac{1}{(1-\phi)^{2.5}}g'(0), \frac{Nu_x}{\sqrt{\mathrm{Re}_x}} = \frac{k_{nf}}{k_f}\left(-\left[1+Rd\theta_w^3\right]\theta'(0)\right) \tag{17}$$

$\mathrm{Re}_x = u_w x/v$ is the Reynolds number.

3. HAM Solution

Liao [46,47] proposed the homotopy analysis technique in 1992. In order to attain this method, he used the ideas of a topology called homotopy. For the derivation he used two homotopic functions, where one of them can be continuously distorted into another. He used Ψ_1, Ψ_2 for binary incessant purposes and X and Y are dual topological plane, additionally, if Ψ_1 and Ψ_2 map from X to Y, then Ψ_1 is supposed to be homotopic to Ψ_2. If a continuous function of ψ is produced:

$$\Psi : X \times [0,\ 1] \to Y \tag{18}$$

So that $x \in X$

$$\Psi[x,\ 0] = \Psi_1(x) \text{ and } \Psi[x,\ 1] = \Psi_2(x) \tag{19}$$

where Ψ is homotopic. Here, we use the HAM to solve Equations (11)–(13), consistent with the boundary restrain (14). The preliminary guesses are selected as follows:

The linear operators are denoted as $L_{\hat{f}}$ and $\mathrm{L}_{\hat{\theta}}$, and are represented as

$$L_{\hat{f}}(\hat{f}) = \hat{f}''', L_{\hat{g}}(\hat{g}) = \mathrm{g}'', \mathrm{L}_{\hat{\theta}}(\hat{\theta}) = \hat{\theta}'' \tag{20}$$

Which has the following applicability:

$$\begin{gathered} L_{\hat{f}}(e_1 + e_2\eta + e_3\eta^2 + e_4\eta^3) = 0, L_{\hat{g}}(e_5 + e_6\eta + e_7\eta^2) = 0 \\ \mathrm{L}_{\hat{\theta}}(e_8 + e_9\eta) = 0 \end{gathered} \tag{21}$$

where the representation of coefficients is included in the general solution by $e_i(i = 1- > 7)$.

The corresponding non-linear operators are sensibly selected as $N_{\hat{f}}$, $N_{\hat{g}}$ and $N_{\hat{\theta}}$, and identify in the form:

$$\begin{gathered} N_{\hat{f}}\left[\hat{f}(\eta;\zeta), \hat{g}(\eta;\zeta)\right] = \frac{1}{(1-\phi)^{2.5}\left((1-\phi)+\phi\frac{(\rho_s)_{CNT}}{\rho_f}\right)}\hat{f}_{\eta\eta\eta} - \frac{\beta_0^2}{\lambda}\hat{f}_{\eta\eta} - \frac{\mu_{nf}}{(1-\phi)^{2.5}k^*b}\hat{f}_{\eta\eta} \\ -\left[\lambda\left(\hat{f}_{\eta\eta} + \frac{\eta}{2}\hat{f}_{\eta\eta\eta}\right) + \hat{f}_\eta\hat{f}_{\eta\eta} - \hat{f}\hat{f}_{\eta\eta} - 2\frac{\Omega}{b}\hat{g}_\eta\right] \end{gathered} \tag{22}$$

$$\begin{gathered} N_{\hat{g}}\left[\hat{f}(\eta;\zeta), \hat{g}(\eta;\zeta)\right] = \frac{1}{(1-\phi)^{2.5}\left((1-\phi)+\phi\frac{(\rho_s)_{CNT}}{\rho_f}\right)}\hat{g}_{\eta\eta\eta} - \frac{\beta_0^2}{\lambda}\hat{g}_\eta + \frac{\mu_{nf}}{(1-\phi)^{2.5}k^*b}\hat{g}_\eta \\ -\left[\lambda(\hat{g}_\eta + \frac{\eta}{2}\hat{g}_{\eta\eta}) + \hat{g}\hat{f}_{\eta\eta} - \hat{f}\hat{g}_{\eta\eta} - 2\frac{\Omega}{b}\hat{f}_{\eta\eta}\right] \end{gathered} \tag{23}$$

$$\begin{gathered} N_{\hat{\theta}}\left[\hat{f}(\eta;\zeta), \hat{g}(\eta,\zeta), \hat{\theta}(\eta;\zeta)\right] = \hat{\theta}_{\eta\eta} + R\left[\left(1+(\theta_w-1)\hat{\theta}\right)^3\hat{\theta}_{\eta\eta} + 3\left(1+(\theta_w-1)\hat{\theta}\right)^2(\theta_w-1)\hat{\theta}_\eta^2\right] \\ +\frac{Ec}{\mathrm{Pr}}\left(\hat{f}_{\eta\eta}^2 + \hat{g}_\eta^2\right) - \frac{1}{\mathrm{Pr}}\left[\lambda\frac{\eta}{2}\hat{\theta}_\eta - f\hat{\theta}_\eta\right] \end{gathered} \tag{24}$$

For Equations (8–10), the $0th$-order scheme takes the form

$$(1-\zeta)L_{\hat{f}}\left[\hat{f}(\eta;\zeta) - \hat{f}_0(\eta)\right] = p\hbar_{\hat{f}}N_{\hat{f}}\left[\hat{f}(\eta;\zeta), \hat{g}(\eta;\zeta)\right] \tag{25}$$

$$(1-\zeta)L_{\hat{g}}[\hat{g}(\eta;\zeta)-\hat{g}_0(\eta)] = p\hbar_{\hat{g}}N_{\hat{g}}\left[\hat{f}(\eta;\zeta),\hat{g}(\eta;\zeta)\right] \tag{26}$$

$$(1-\zeta)\ L_{\hat{\theta}}\left[\hat{\theta}(\eta;\zeta)-\hat{\theta}_0(\eta)\right] = p\hbar_{\hat{\theta}}N_{\hat{\theta}}\left[\hat{f}(\eta;\zeta),\hat{g}(\eta;\zeta),\hat{\theta}(\eta;\zeta)\right] \tag{27}$$

where the boundary constrains are:

$$\begin{array}{l}\hat{f}(\eta;\zeta)\Big|_{\eta=0}=0,\ \frac{\partial\hat{f}(\eta;\zeta)}{\partial\eta}\Big|_{\eta=0}=1,\ \hat{g}(\eta;\zeta)|_{\eta=0}=0\\ \hat{\theta}(\eta;\zeta)\big|_{\eta=0}=1,\ \frac{\partial\hat{f}(\eta;\zeta)}{\partial\eta}\Big|_{\eta\to\infty}\to 0,\ \hat{g}(\eta;\zeta)|_{\eta\to\infty}\to 0\\ \hat{f}(\eta;\zeta)\Big|_{\eta\to\infty}\to 0,\ \hat{\theta}(\eta;\zeta)\big|_{\eta\to\infty}\to 0.\end{array} \tag{28}$$

where the embedding restriction is $\zeta\in[0,1]$, to normalize for the solution convergence $\hbar_{\hat{f}}$, $\hbar_{\hat{g}}$ and $\hbar_{\hat{\theta}}$ are used. When $\zeta=0$ and $\zeta=1$, we get:

$$\hat{f}(\eta;1)=\hat{f}(\eta),\hat{g}(\eta;1)=\hat{g}(\eta),\hat{\theta}(\eta;1)=\hat{\theta}(\eta) \tag{29}$$

Expanding $\hat{f}(\eta;\zeta),\hat{g}(\eta;\zeta)$ and $\hat{\theta}(\eta;\zeta)$ through Taylor's series for $\zeta=0$,

$$\begin{array}{rcl}\hat{f}(\eta;\zeta) &=& \hat{f}_0(\eta)+\sum_{n=1}^{\infty}\hat{f}_n(\eta)\zeta^n\\ \hat{g}(\eta;\zeta) &=& \hat{g}_0(\eta)+\sum_{n=1}^{\infty}\hat{g}_n(\eta)\zeta^n\\ \hat{\theta}(\eta;\zeta) &=& \hat{\theta}_0(\eta)+\sum_{n=1}^{\infty}\hat{\theta}_n(\eta)\zeta^n.\end{array} \tag{30}$$

$$\hat{f}_n(\eta)\ =\ \frac{1}{n!}\frac{\partial\hat{f}(\eta;\zeta)}{\partial\eta}\Bigg|_{p=0},\hat{g}_n(\eta)\ =\ \frac{1}{n!}\frac{\partial\hat{g}(\eta;\zeta)}{\partial\eta}\Bigg|_{p=0},\ \hat{\theta}_n(\eta)\ =\ \frac{1}{n!}\frac{\partial\hat{\theta}(\eta;\zeta)}{\partial\eta}\Bigg|_{p=0}. \tag{31}$$

The boundary constrains are:

$$\hat{f}_w(0)=\hat{f}_w{}'(0)=\hat{g}(0)=0,\hat{\theta}_w(0)=0,\mathrm{at}\eta=0 \tag{32}$$

$$\hat{f}'_w(\infty)=\hat{g}_w(\infty)=\hat{\theta}_w(\gamma)=\hat{f}_w(\infty)\to 0\mathrm{at}\eta\to\infty. \tag{33}$$

Resulting in:

$$\begin{array}{l}\Re_n^{\hat{f}}(\eta)=\frac{1}{(1-\phi)^{2.5}\left((1-\phi)+\phi\frac{(\rho_s)_{CNT}}{\rho_f}\right)}\hat{f}_{n-1}^{iv}-\frac{\beta_0^2}{\lambda}\hat{f}''_{n-1}-\frac{\mu_{nf}}{(1-\phi)^{2.5}k^*b}\hat{f}''_{n-1}\\ -\left[\lambda\left(\hat{f}''_{n-1}+\frac{\eta}{2}\hat{f}'''{}_{n-1}\right)+\sum\limits_{j=0}^{w-1}\hat{f}'_{w-1-j}\hat{f}''{}_j-\sum\limits_{j=0}^{w-1}\hat{f}_{w-1-j}\hat{f}''{}_j-2\frac{\Omega}{b}\hat{g}'_{n-1}\right]\end{array} \tag{34}$$

$$\begin{array}{l}\Re_n^{\hat{g}}(\eta)=\frac{1}{(1-\phi)^{2.5}\left((1-\phi)+\phi\frac{(\rho_s)_{CNT}}{\rho_f}\right)}\hat{g}'''_{n-1}-\frac{\beta_0^2}{\lambda}\hat{g}'_{n-1}+\frac{\mu_{nf}}{(1-\phi)^{2.5}k^*b}\hat{g}'_{n-1}\\ -\left[\lambda\left(\hat{g}'_{n-1}+\frac{\eta}{2}\hat{g}''_{n-1}\right)+\sum\limits_{j=0}^{w-1}g_{w-1-j}\hat{f}''_j-\sum\limits_{j=0}^{w-1}f_{w-1-j}\hat{g}''_j-2\frac{\Omega}{b}\hat{f}''_{n-1}\right]\end{array} \tag{35}$$

$$\begin{array}{l}R_n^{\hat{\theta}}(\eta)=\left(\hat{\theta}''{}_{n-1}\right)+R\left[\left(1+(\theta_w-1)\hat{\theta}_{n-1}\right)^3\hat{\theta}''{}_{n-1}+3(\theta_w-1)\left(1+(\theta_w-1)\hat{\theta}_{n-1}\right)^2\hat{\theta}'{}_{n-1}\right]+\frac{Ec}{\Pr}\left(\hat{f}''^2+\hat{g}'^2\right)\\ -\frac{1}{\Pr}\left[\lambda\frac{\eta}{2}\hat{\theta}'{}_{n-1}-\hat{f}\hat{\theta}'{}_{n-1}\right]\end{array} \tag{36}$$

where

$$\chi_n=\begin{cases}0, & \text{if } \zeta\le 1\\ 1, & \text{if } \zeta>1.\end{cases} \tag{37}$$

4. Results and Discussion

In this section, we described the physical resources of the modeled problems and their impact on $f'(\eta)$, $g(\eta)$, and $\theta(\eta)$, which are identified in Figures 1–13. In Figure 1, a graphical representation of the problem is shown.

4.1. Velocity Profile $f'(\eta)$ and $g(\eta)$

The influence of Ω, β, ϕ and λ on the velocity profile is presented in Figures 1–8. The impact of Ω on $f'(\eta)$ and $g(\eta)$ is presented in Figures 1 and 2. For greater values of Ω, $f'(\eta)$ is increased. Actually, increasing the rotation parameter increases kinetic energy, which in result augmented the velocity profile. Indeed, $g(\eta)$ is decreased due to a greater rotation parameter rate, as compared to the stretching rate, which had a greater rotation rate for a larger value of Ω. Hence, the velocity field increases for larger rotation effects. Figures 3 and 4 represent the influence of ϕ on the $f'(\eta)$ and $g(\eta)$ profile. With an increase in ϕ, the velocity profile decreases. It is examined that $f'(\eta)$ and $g(\eta)$ decrease uniformly in nanofluids with a rise in ϕ. This is due to the detail that an increase in the ϕ increases the density of the nanofluid and this results in equally slowing the fluid $f'(\eta)$ and $g(\eta)$ profiles. Figures 5 and 6 describe the effect of λ on $f'(\eta)$ and $g(\eta)$. It is defined in the figures that with increases in λ, the velocity profiles decrease consistently. It is also indicated from the figures that the velocity profiles intensify for rising λ, while we can examine an opposing influence of λ on $f'(\eta)$ and $g(\eta)$ inside the nanofluid and in the thickness of the layer. Figures 7 and 8 represent the influence of β on $f'(\eta)$ and $g(\eta)$. With increases in β, the velocity profiles of fluid film decrease consistently. It was also detected that a rise in β resulted in a decrease in the fluid profiles $f'(\eta)$ and $g(\eta)$ of the nanofluid, as well as for the layer thickness. The purpose behind such an influence of β is for the stimulation of a delaying body force, stated as Lorentz force, due to the presence of β in an electrically conducting nanofluid layer. Since β suggests the ratio of hydromagnetic body force and viscous force, a larger value of β specifies a stronger hydromagnetic body force, which has a trend to slow the fluid flow.

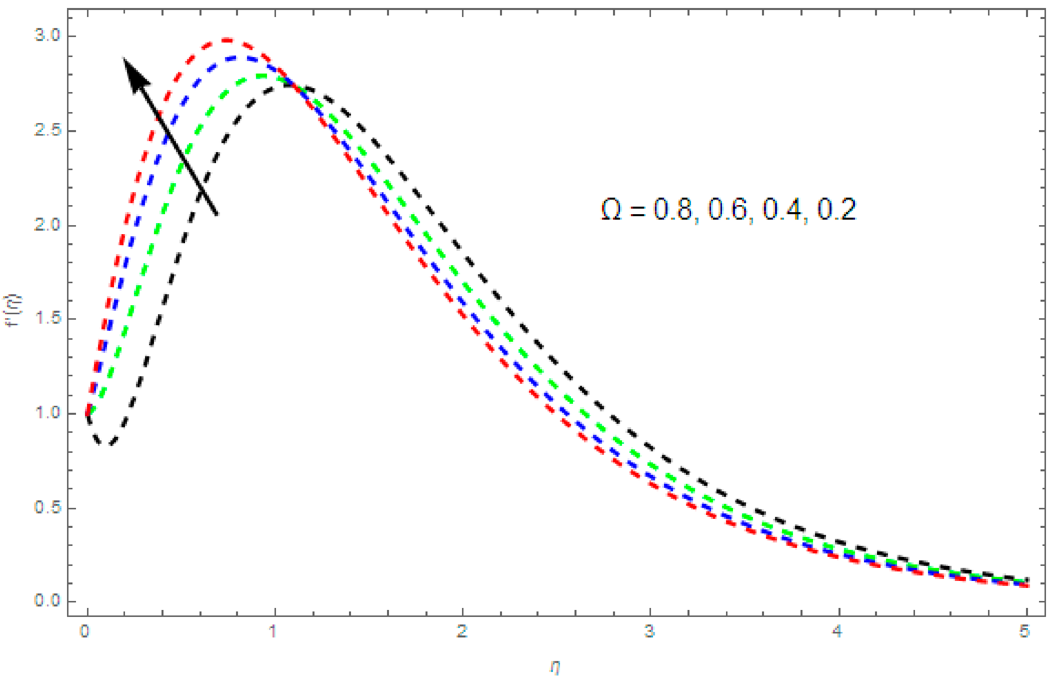

Figure 1. The influence of the rotation parameter Ω on $f'(\eta)$ when $\beta = 0.2, \phi = 0.1, \lambda = 0.3$.

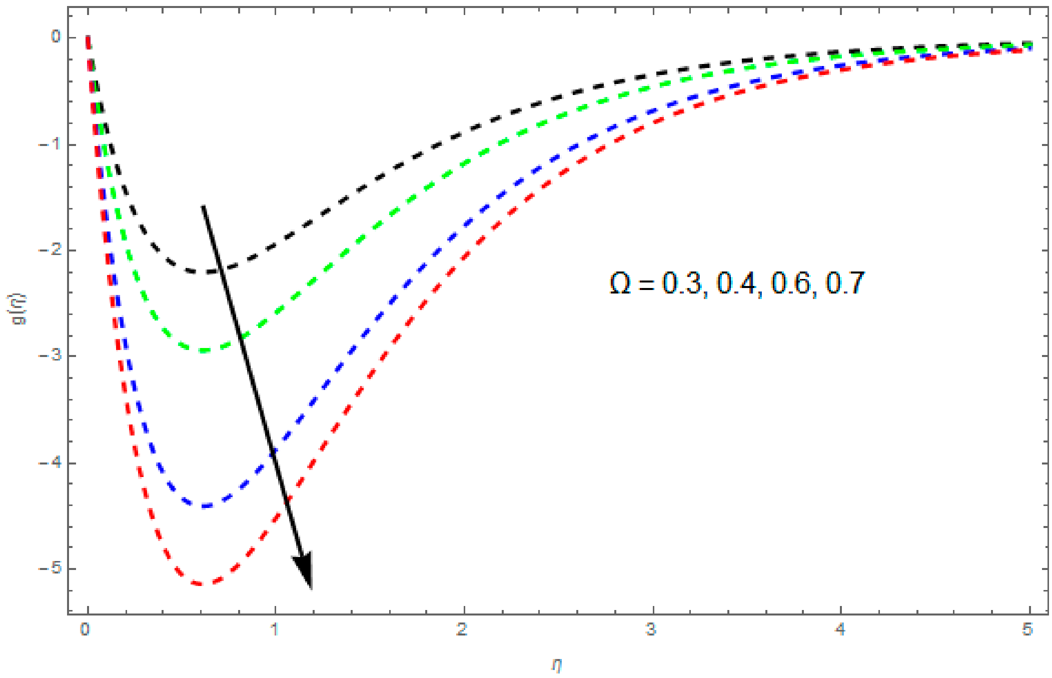

Figure 2. The effect of the rotation rate parameter Ω on $g(\eta)$ when $\beta = 0.2, \phi = 0.1, \lambda = 0.7$.

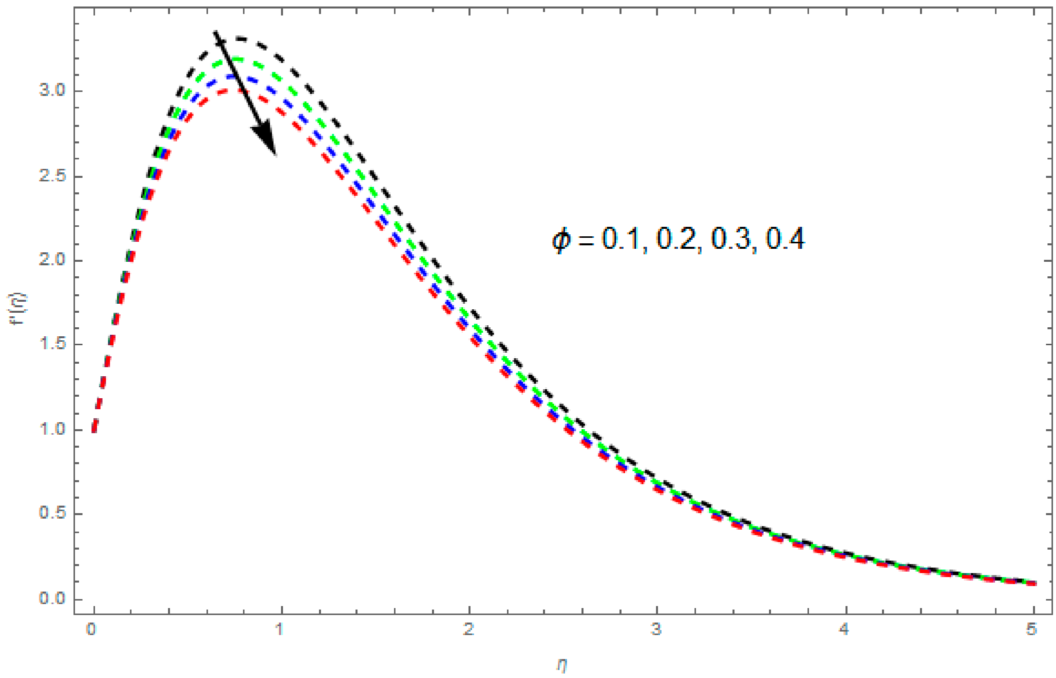

Figure 3. The effect of nanoparticle volume friction ϕ on $f'(\eta)$ when $\beta = 0.9, \lambda = 0.5, \Omega = 0.1$.

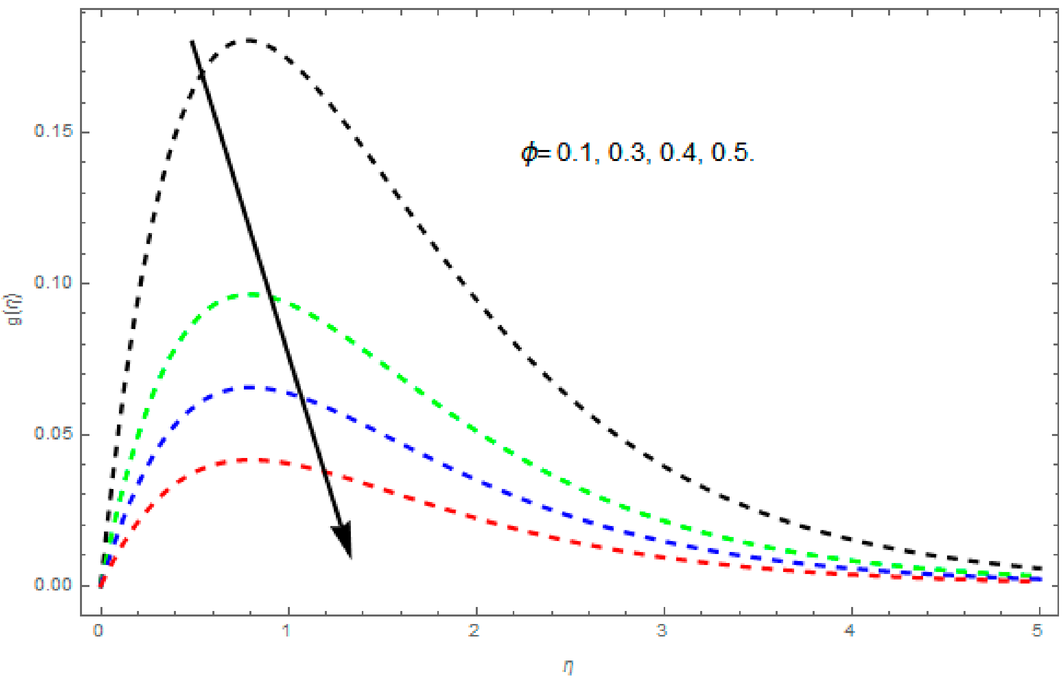

Figure 4. The impact of nanoparticle volume friction ϕ on $g(\eta)$ when $\beta = 0.1, \lambda = 0.2, \Omega = 0.7$.

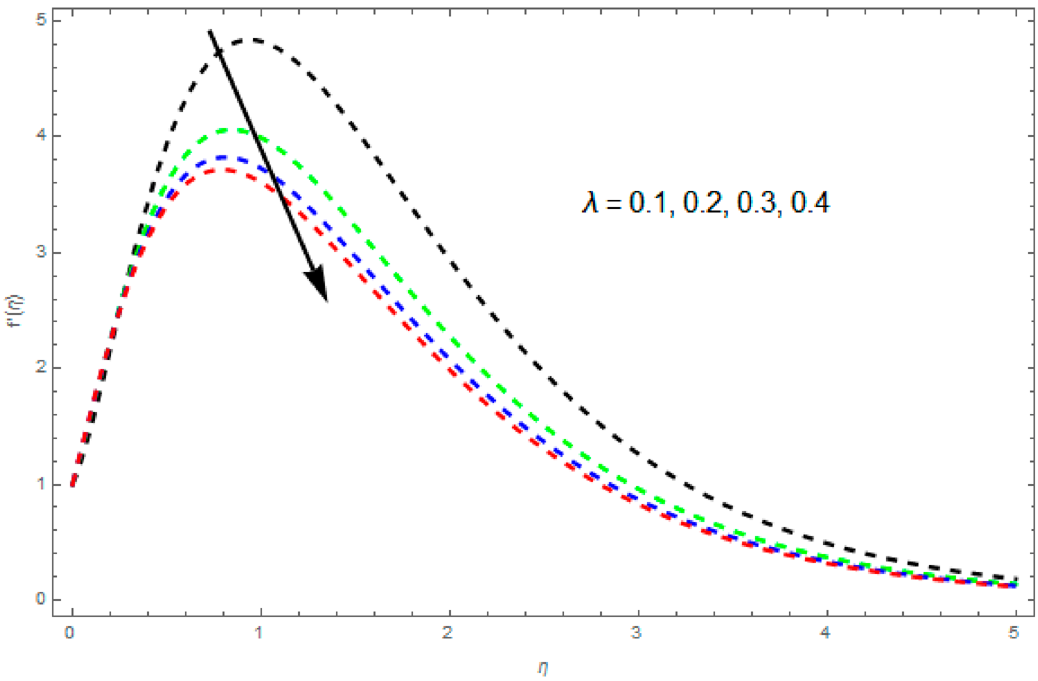

Figure 5. The influence of the unsteadiness parameter λ on $f'(\eta)$ when $\beta = 0.9, \phi = 0.1, \Omega = 0.1$.

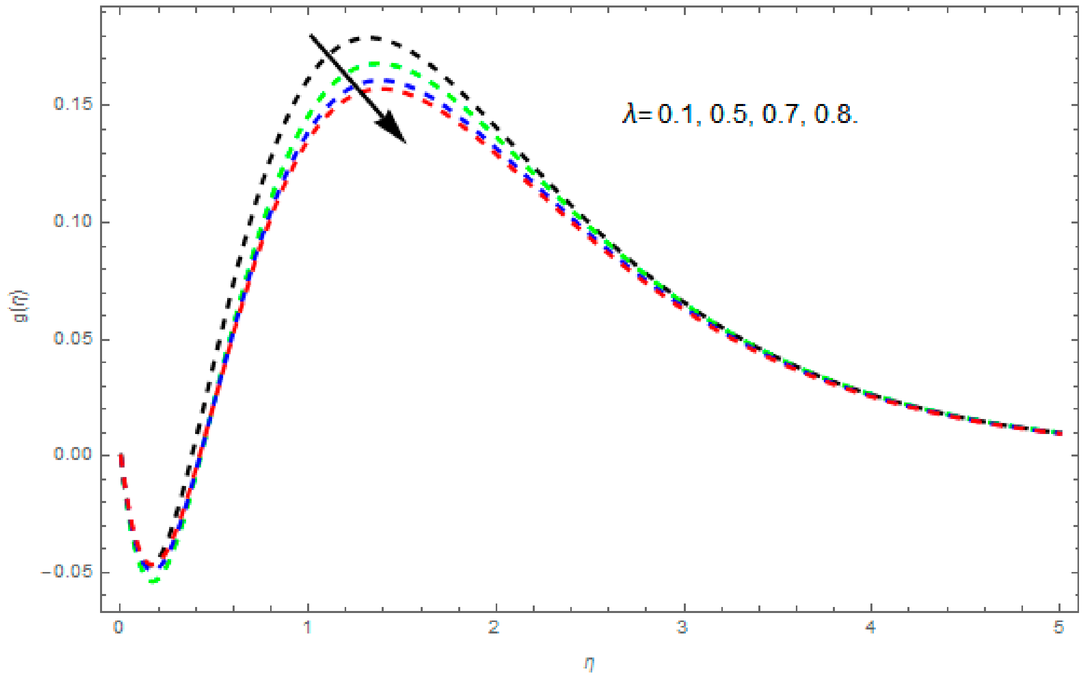

Figure 6. The effect of the unsteadiness parameter λ on $g(\eta)$ when $\beta = 0.2, \phi = 0.1, \Omega = 0.2$.

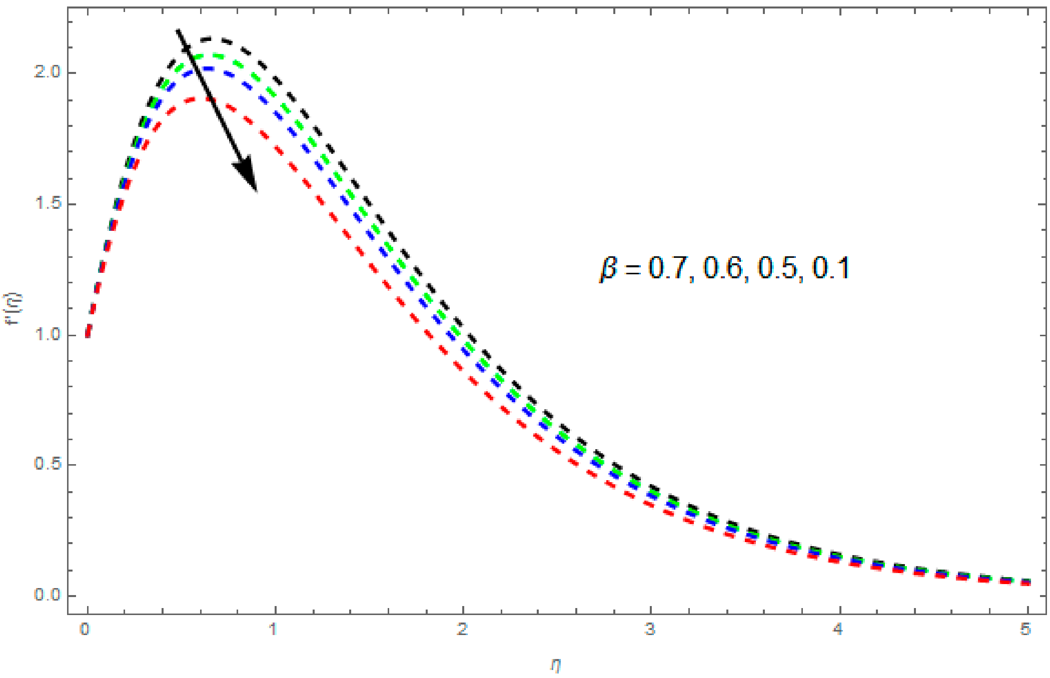

Figure 7. The effect of magnetic field β on $f'(\eta)$ when $\lambda = 0.2, \phi = 0.1, \Omega = 0.1$.

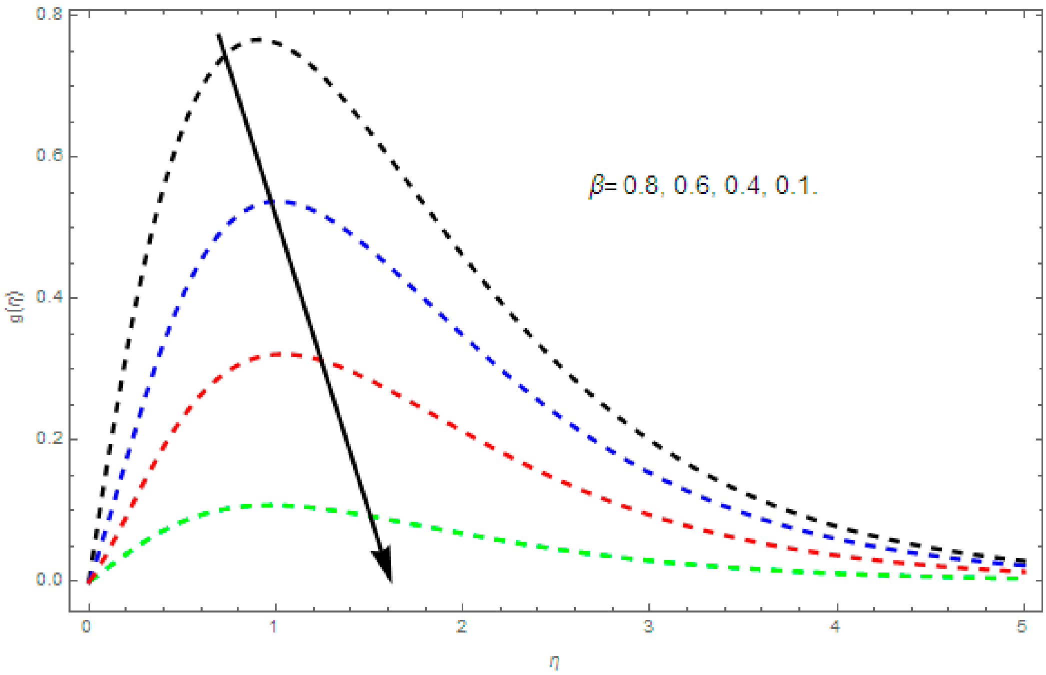

Figure 8. The effect of magnetic field β on $g(\eta)$ when $\lambda = 0.7, \phi = 0.1, \Omega = 0.1$.

4.2. *Temperature Profile* $\theta(\eta)$

The impact of $\theta(\eta)$ on physical parameters λ, Ec, θ_w, Rd and Pr is defined in Figures 9–13. Figure 9 represent the impact of λ on the $\theta(\eta)$ profile. Figure 9 represents that the increase in the λ momentum boundary layer thickness decreases. Figures 10 and 11 disclosed the responses of $\theta(\eta)$ for θ_w and Rd. The influence of Rd on $\theta(\eta)$ is presented in Figure 11. By increasing Rd, the temperature of the nanofluid boundary layer area is increased. It is observed in Figure 11 that $\theta(\eta)$ is augmented with a rise in the Rd. An enhanced Rd parameter leads to a release of heat energy in the flow direction, therefore the fluid $\theta(\eta)$ is increased. Graphical representation identifies that $\theta(\eta)$ is increased when we increase the ratio strength and thermal radiation temperature. The impact of $\theta(\eta)$ on Pr is given in Figure 12, where $\theta(\eta)$ decreases with large value of Pr and for smaller value increases. The variation of $\theta(\eta)$ for the variation of Pr is illustrated such that Pr specifies the ratio of momentum diffusivity to thermal diffusivity. It is realized that $\theta(\eta)$ is reduced with a rising Pr. Moreover, by suddenly rising Pr, the thermal boundary layer thickness decreases. Figure 13 identifies that for increasing Ec, the $\theta(\eta)$ attainment is enlarged, which supports the physics. By increasing Ec, the heat stored in the liquid is dissipated, due to the enhanced temperature, whereas $\theta(\eta)$ increases with increasing values of the Eckert number and the thermal boundary layer thickness of the nanofluid becomes larger.

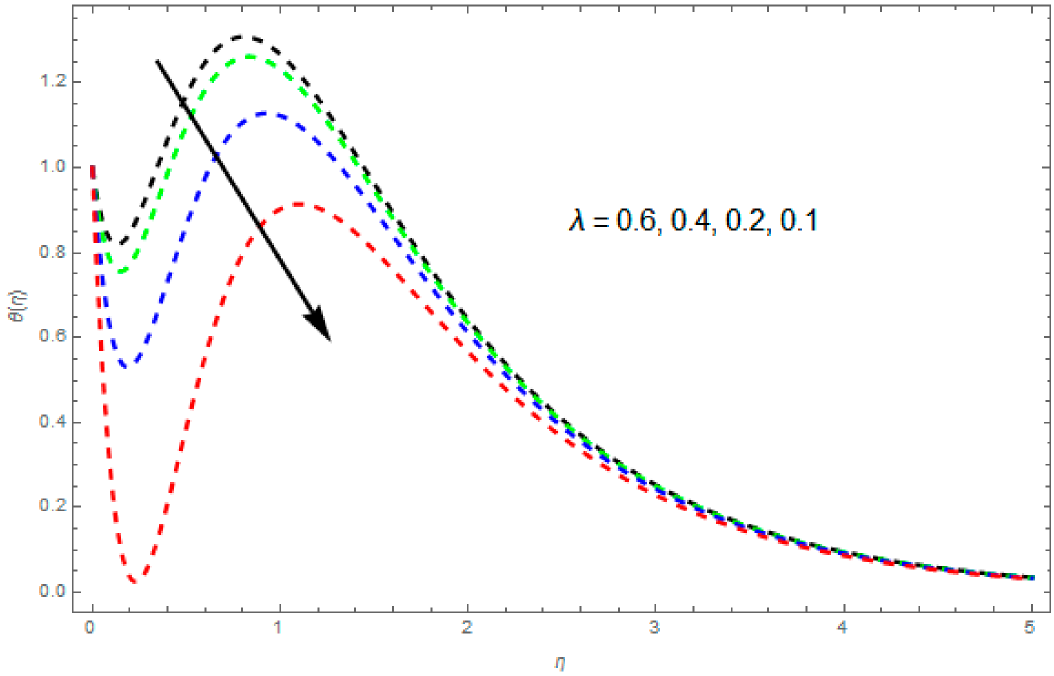

Figure 9. The effect of the unsteadiness parameter (λ) on $\theta(\eta)$ when $Rd = 0.1, Ec = 0.2, Pr = 7, \theta_w = 1.2$.

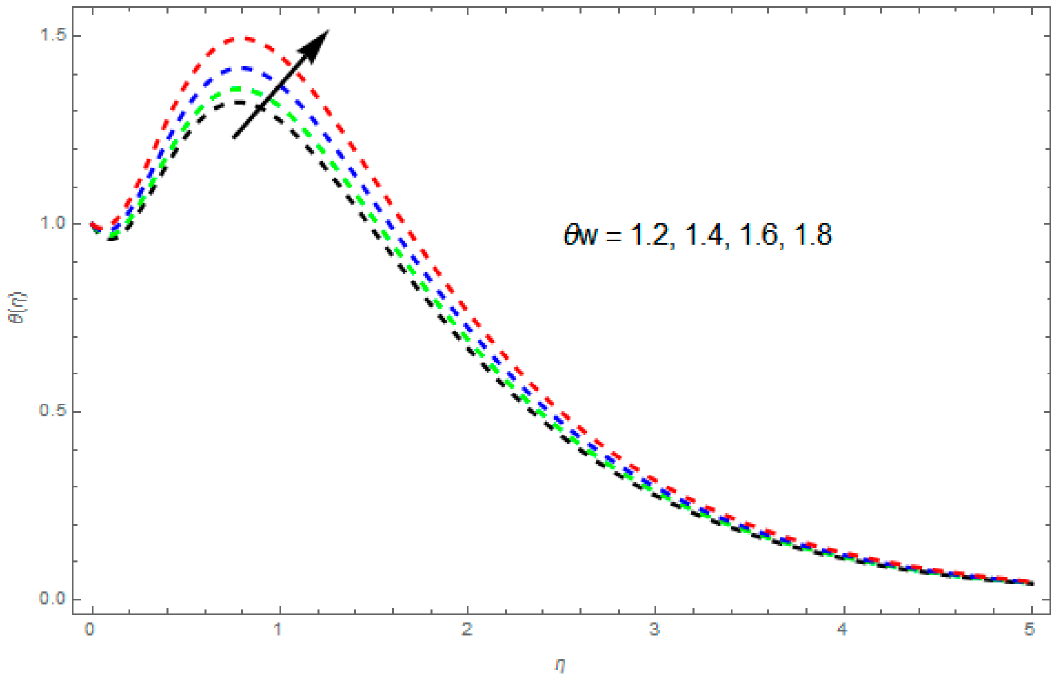

Figure 10. The influence of the temperature ratio parameter on $\theta(\eta)$ when $Rd = 0.5, \lambda = 0.6, \mathrm{Pr} = 6.6, Ec = 0.2$.

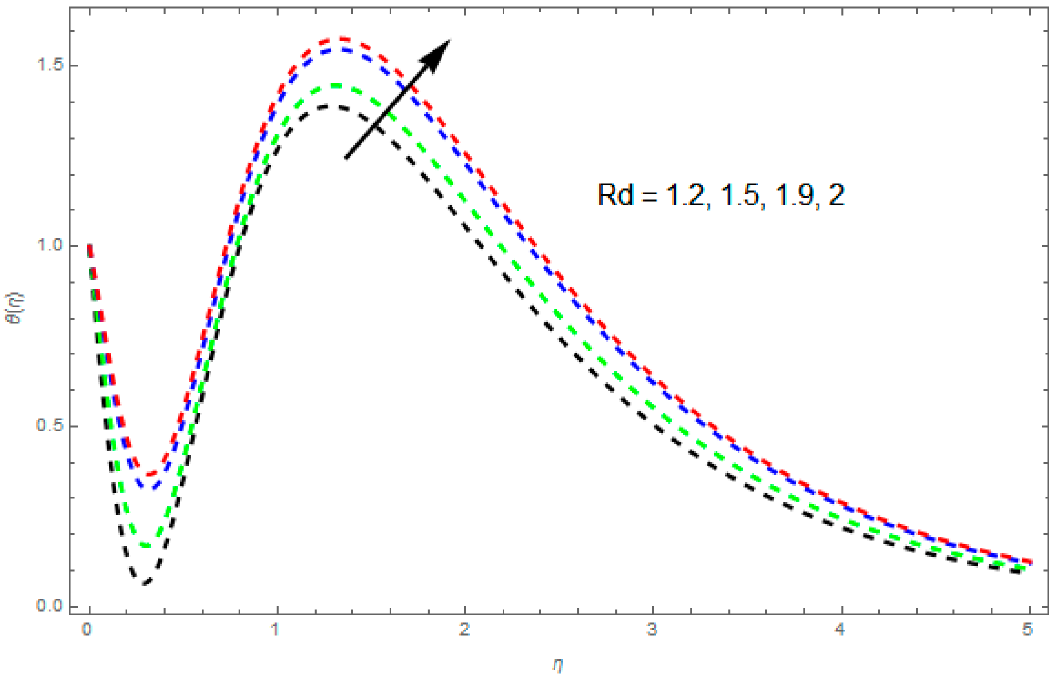

Figure 11. The influence of the radiation parameter (Rd) on $\theta(\eta)$ when $\theta_w = 0.5, \lambda = 0.6, \mathrm{Pr} = 6.6, Ec = 0.6$.

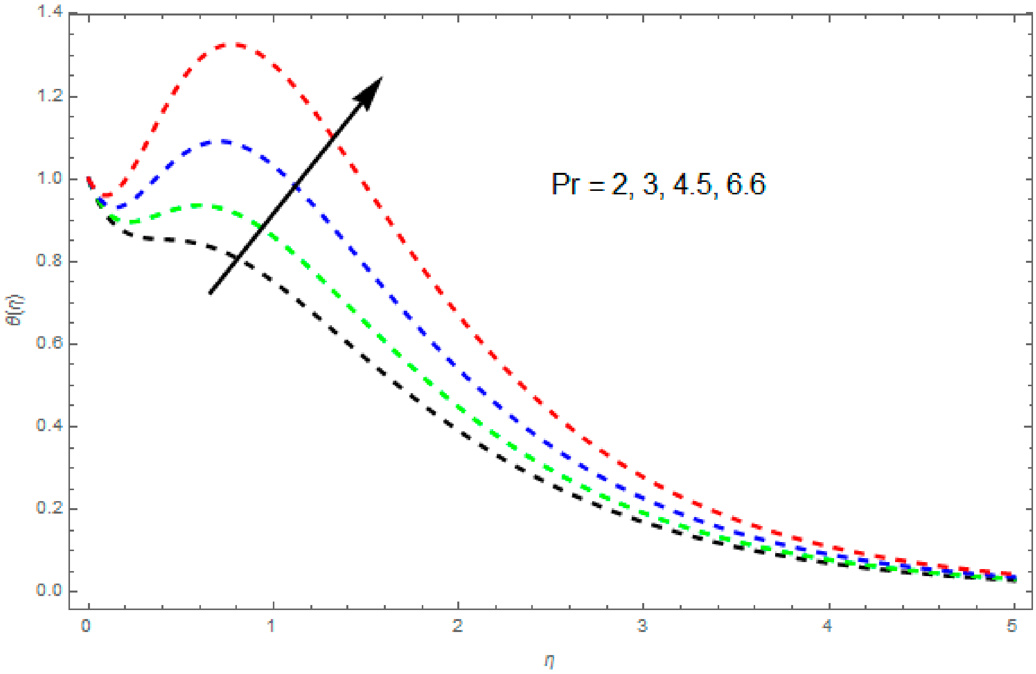

Figure 12. The influence of Prandtl number (Pr) on $\theta(\eta)$ when $Rd = 0.5, \lambda = 0.6, \theta_w = 6.6, Ec = 0.2$.

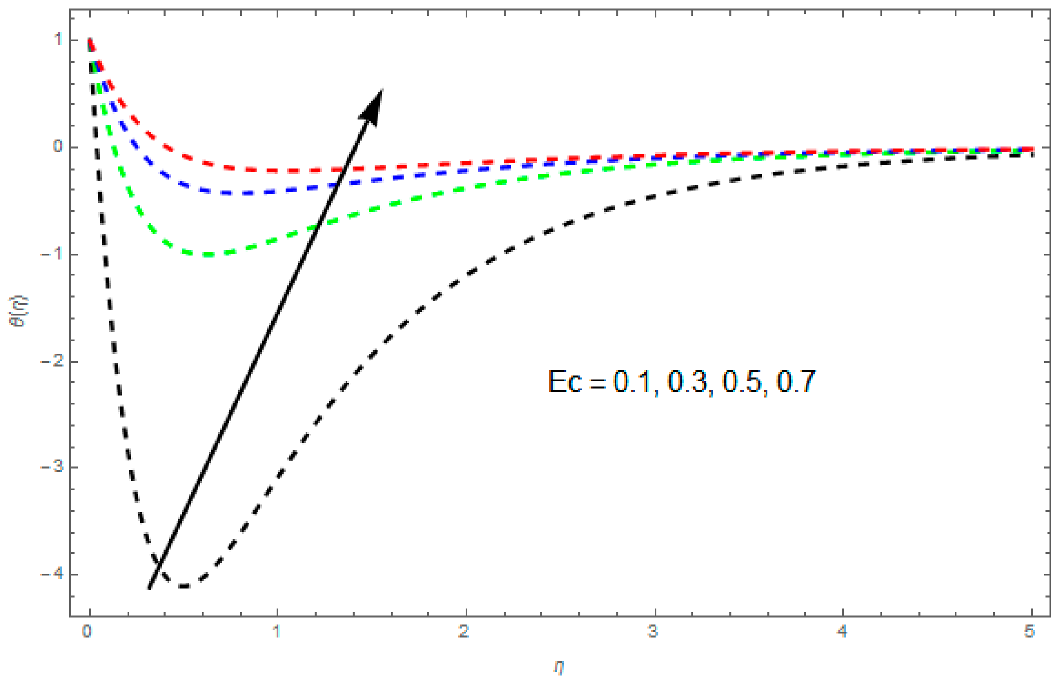

Figure 13. The impact of the Eckert number (Ec) on $\theta(\eta)$ when $Rd = 0.4, \lambda = 0.6, \theta_w = 0.6, \mathrm{Pr} = 1.8$.

4.3. Table Discussion

The effect of skin friction in the x and y directions is shown in Table 1, due to change of parameters ϕ, β, λ, ρ_s and ρ_f. We can see in Table 1 that the skin friction coefficient rises with rising values of λ,β, ρ_s and ϕ. The skin friction coefficient decreases with increasing values of ρ_f, as shown in Table 1. The impact of $Rd, \theta_w, \mathrm{Pr}$ and Ec on $-\frac{knf}{kf}\left[1 + Rd\theta_w^3\right]\theta'(0)$ are calculated numerically. It was detected that a higher value of Rd and θ_w increases the heat flux, while a higher value of Pr and Ec decreases it, as shown in Table 2. Some physical properties of CNTs are shown in Tables 3 and 4.

Table 1. Skin friction $f''(0)$ versus various values of embedded parameters.

ϕ	β	λ	ρ_s	ρ_f	C_{fx}	C_{fy}
0.1	0.3	0.5	0.4	0.4	1.80946	1.80946
0.3					2.36646	2.36646
0.5					3.23183	3.23183
0.1	0.1				1.80946	1.80946
	0.3				1.83280	1.83280
	0.5				1.86280	1.86280
	0.1	0.1			1.80946	1.80946
		0.3			1.81835	1.81835
		0.5			1.82867	1.82867
		0.1	0.1		1.80946	1.80946
			0.3		1.82759	1.82759
			0.5		1.84571	1.84571
			0.1	0.1	1.80946	1.80946
				0.3	1.79496	1.79496
				0.5	1.78530	1.78530

Table 2. Nusslet number versus various values of embedded parameters.

R	θ_w	Pr	Ec	$-\frac{knf}{kf}[1+Rd\theta_w^3]\theta'(0)$
0.1	0.5	0.7	0.6	0.408170
0.3				0.452415
0.5				0.497617
0.1	0.1			0.408170
	0.3			0.418514
	0.5			0.429786
	0.1	0.1		0.408170
		0.3		0.401541
		0.5		0.393572
		0.1	0.1	0.408170
			0.3	0.420824
			0.5	0.430319

Table 3. Thermophysical properties of different base fluids and carbon nanotubes (CNTs).

Physical Properties	Base Fluid	Nanoparticles	
	Water/Ethylene Glycol)	SWCNT	MWCNT
$\rho(kg/m^3)$	=	2,600	1,600
$c_p(J/kgK)$	=	425	796
$k(W/mK)$	=	6,600	3,000

Table 4. Variation of thermal conductivities of CNT nanofluids with the diameter of CNTs.

Diameter of CNTs	Thermal Conductivity of Nanofluids
50 mm	1.077
200 μm	1.078
20 μm	1.083
5 μm	1.085
50 nm	1.085
500 pm	1.087

5. Conclusions

Exploration on nanoparticle presentation has established more deliberation in mechanical and industrial engineering, due to the probable uses of nanoparticles in cooling devices to produce an increase in continuous phase fluid thermal performance. The radiation phenomena acts as a source of energy to the fluid system. In this research, the time dependent rotating single-wall electrically conducting carbon nanotubes with aqueous suspensions under the influence of nonlinear thermal radiation in a permeable medium was investigated. The basic governing equations, in the form of partial differential equations (PDEs), were transformed into to a set of ordinary differential equations (ODEs) suitable for transformations. The optimal approach was used for the solution. The main concluding points are given below:

- The thermal boundary layer thickness is reduced by a greater rotation rate parameter.
- Velocity and temperature profile decrease due to increases in the unsteadiness parameter.
- A greater ϕ increases the asset of frictional force within a fluid motion.
- The heat transfer rate rises for greater Rd and θ_w values.
- The skin friction coefficient increases with increasing values of ϕ and β.
- A greater value of Rd and θ_w increases the heat flux, while a greater value of Pr and Ec decreases it.
- By enhancing Pr, $\theta(\eta)$ is reduced.

Author Contributions: M.J. and Z.S. modeled the problem and wrote the manuscript. S.I., I.T. and I.K. thoroughly checked the mathematical modeling and English corrections. W.K. and Z.S. solved the problem using Mathematica software. M.J., J.M. and I.T. contributed to the results and discussions. All authors finalized the manuscript after its internal evaluation.

Acknowledgments: The fourth author would like to thank Deanship of Scientific Research, Majmaah University for supporting this work under the Project Number No 1440-43.

Conflicts of Interest: The authors declare no conflict of interest.

References

1. Khan, W.A. Buongiorno model for nanofluid Blasius flow with surface heat and mass fluxes. *J. Thermophys. Heat Transf.* **2013**, *27*, 134–141. [CrossRef]
2. Mahdy, A.; Chamkha, A. Heat transfer and fluid flow of a non-Newtonian nano fluid over an unsteady contracting cylinder employing Buongiorno'smodel. *Int. J. Numer. Method Heat Fluid Flow* **2015**, *25*, 703–723. [CrossRef]
3. Malvandi, A.; Moshizi, S.A.; Soltani, E.G.; Ganji, D.D. Modified Buongiorno's model for fully developed mixed convection flow of nanofluids in a vertical annular pipe. *Comput. Fluids* **2014**, *89*, 124–132. [CrossRef]
4. Hayat, T.; Ashraf, M.B.; Shehzad, S.A.; Abouelmaged, E.I. Three dimensional flow of Erying powell nanofluid over an exponentially stretching sheet. *Int. J. Numer. Method Heat Fluid Flow* **2015**, *25*, 333–357. [CrossRef]
5. Nadeem, S.; Haq, R.U.; Akbar, N.S.; Lee, C.; Khan, Z.H. Numerical study of boundary layer flow and heat transfer of Oldroyed-B nanofluid towards a stretching sheet. *PLoS ONE* **2013**, *8*, e69811. [CrossRef] [PubMed]
6. Rosmila, A.B.; Kandasamy, R.; Muhaimin, I. Lie symmetry groups transformation for MHD natural convection flow of nanofluid over linearly porous stretching sheet in presence of thermal stratification. *Appl. Math. Mech. Engl. Ed.* **2012**, *33*, 593–604. [CrossRef]
7. Ellahi, R. The effects of MHD an temperature dependent viscosity on the flow of non-Newtonian nanofluid in a pipe analytical solutions. *Appl. Math. Model.* **2013**, *37*, 1451–1467. [CrossRef]
8. Nadeem, S.; Saleem, S. Series solution of unsteady Erying Powell nanofluid flow on a rotating cone. *Indian J. Pure Appl. Phys.* **2014**, *52*, 725–737.
9. Abolbashari, M.H.; Freidoonimehr, N.; Rashidi, M.M. Analytical modeling of entropy generation for Casson nano-fluid flow induced by a stretching surface. *Adv. Powder Technol.* **2015**, *6*, 542–552. [CrossRef]
10. Choi, S.U.S.; Siginer, D.A.; Wang, H.P. Enhancing thermal conductivity of fluids with nanoparticle developments and applications of non-Newtonian flows. *ASME N. Y.* **1995**, *66*, 99–105.
11. Buongiorno, J. Convective transport in nanofluids. *ASME J Heat Transf.* **2005**, *128*, 240–250. [CrossRef]
12. Kumar, K.G.; Rudraswamy, N.G.; Gireesha, B.J.; Krishnamurthy, M.R. Influence of nonlinear thermal radiation and viscous dissipation on three-dimensional flow of Jeffrey nanofluid over a stretching sheet in the presence of Joule heating. *Nonlinear Eng.* **2017**, *6*, 207–219.
13. Rudraswamy, N.G.; Shehzad, S.A.; Kumar, K.G.; Gireesha, B.J. Numerical analysis of MHD three-dimensional Carreau nanoliquid flow over bidirectionally moving surface. *J. Braz. Soc. Mech. Sci. Eng.* **2017**, *23*, 5037–5047. [CrossRef]
14. Gireesha, B.J.; Kumar, K.G.; Ramesh, G.K.; Prasannakumara, B.C. Nonlinear convective heat and mass transfer of Oldroyd-B nanofluid over a stretching sheet in the presence of uniform heat source/sink. *Results Phys.* **2018**, *9*, 1555–1563. [CrossRef]
15. Kumar, K.G.; Gireesha, B.J.; Manjunatha, S.; Rudraswamy, N.G. Effect of nonlinear thermal radiation on double-diffusive mixed convection boundary layer flow of viscoelastic nanofluid over a stretching sheet. *IJMME* **2017**, *12*, 18.
16. Nadeem, S.; Rehman, A.U.; Mehmood, R. Boundary layer flow of rotating two phase nanofluid over a stretching surface. *Heat Transf. Asian Res.* **2016**, *45*, 285–298. [CrossRef]
17. Mabood, F.; Ibrahim, S.M.; Khan, W.A. Framing the features of Brownian motion and thermophoresis on radiative nanofluid flow past a rotating stretching sheet with magnetohydrodynamics. *Results Phys.* **2016**, *6*, 1015–1023. [CrossRef]
18. Shah, Z.; Islam, S.; Gul, T.; Bonyah, E.; Khan, M.A. The electrical MHD and hall current impact on micropolar nanofluid flow between rotating parallel plates. *Results Phys.* **2018**, *9*, 1201–1214. [CrossRef]

19. Shah, Z.; Gul, T.; Khan, A.M.; Ali, I.; Islam, S. Effects of hall current on steady three dimensional non-newtonian nanofluid in a rotating frame with brownian motion and thermophoresis effects. *J. Eng. Technol.* **2017**, *6*, 280–296.
20. Gireesha, B.J.; Ganesh, K.; Krishanamurthy, M.R.; Rudraswamy, N.G. Enhancement of heat transfer in an unsteady rotating flow for the aqueous suspensions of single wall nanotubes under nonlinear thermal radiation. *Numer. Study* **2018**. [CrossRef]
21. Ishaq, M.; Ali, G.; Shah, Z.; Islam, S.; Muhammad, S. Entropy Generation on Nanofluid Thin Film Flow of Eyring–Powell Fluid with Thermal Radiation and MHD Effect on an Unsteady Porous Stretching Sheet. *Entropy* **2018**, *20*, 412. [CrossRef]
22. Sarit, K.D.; Stephen, U.S.; Choi Wenhua, Y.U.; Pradeep, T. *Nanofluids Science and Technology*; Wiley-Interscience: New Your, NY, USA, 2007; Volume 397.
23. Wong, K.F.V.; Leon, O.D. Applications of nanofluids: Current and future. *Adv. Mech. Eng.* **2010**, *2*, 519659. [CrossRef]
24. Sheikholeslami, M.; Haq, R.L.; Shafee, A.; Zhixiong, L. Heat transfer behavior of Nanoparticle enhanced PCM solidification through an enclosure with V shaped fins. *Int. J. Heat Mass Transf.* **2019**, *130*, 1322–1342. [CrossRef]
25. Sheikholeslami, M.; Gerdroodbary, M.B.; Moradi, R.; Shafee, A.; Zhixiong, L. Application of Neural Network for estimation of heat transfer treatment of Al2O3-H2O nanofluid through a channel. *Comput. Methods Appl. Mech. Eng.* **2019**, *344*, 1–12. [CrossRef]
26. Sheikholeslami, M.; Mehryan, S.A.M.; Shafee, A.; Sheremet, M.A. Variable magnetic forces impact on Magnetizable hybrid nanofluid heat transfer through a circular cavity. *J. Mol. Liquids* **2019**, *277*, 388–396. [CrossRef]
27. Yadav, D.; Lee, D.; Cho, H.H.; Lee, J. The onset of double-diffusive nanofluid convection in a rotating porous medium layer with thermal conductivity and viscosity variation: A revised model. *J. Porous Media* **2016**, *19*, 31–46. [CrossRef]
28. Yadav, D.; Nam, D.; Lee, J. The onset of transient Soret-driven MHD convection confined within a Hele-Shaw cell with nanoparticles suspension. *J. Taiwan Inst. Chem. Eng.* **2016**, *58*, 235–244. [CrossRef]
29. Yadav, D.; Lee, J. The onset of MHD nanofluid convection with Hall current effect. *Eur. Phys. J. Plus* **2015**, *130*, 162–184. [CrossRef]
30. Shah, Z.; Dawar, A.; Islam, S.; Khan, I.; Ching, D.L.C. Darcy-Forchheimer Flow of Radiative Carbon Nanotubes with Microstructure and Inertial Characteristics in the Rotating Frame. *Case Stud. Therm. Eng.* **2018**, *12*, 823–832. [CrossRef]
31. Shah, Z.; Bonyah, E.; Islam, S.; Gul, T. Impact of thermal radiation on electrical mhd rotating flow of carbon nanotubes over a stretching sheet. *AIP Adv.* **2019**, *9*, 015115. [CrossRef]
32. Shah, Z.; Dawar, A.; Islam, S.; Khan, I.; Ching, D.L.C.; Khan, Z.A. Cattaneo-Christov model for Electrical MagnetiteMicropoler Casson Ferrofluid over a stretching/shrinking sheet using effective thermal conductivity model. *Case Stud. Therm. Eng.* **2018**. [CrossRef]
33. Dawar, A.; Shah, Z.; Islam, S.; Idress, M.; Khan, W. Magnetohydrodynamic CNTs Casson Nanofl uid and Radiative heat transfer in a Rotating Channels. *J. Phys. Res. Appl.* **2018**, *1*, 017–032.
34. Khan, A.S.; Nie, Y.; Shah, Z.; Dawar, A.; Khan, W.; Islam, S. Three-Dimensional Nanofluid Flow with Heat and Mass Transfer Analysis over a Linear Stretching Surface with Convective Boundary Conditions. *Appl. Sci.* **2018**, *8*, 2244. [CrossRef]
35. Shah, Z.; Islam, S.; Ayaz, H.; Khan, S. Radiative Heat and Mass Transfer Analysis of Micropolar Nanofluid Flow of Casson Fluid between Two Rotating Parallel Plates with Effects of Hall Current. *ASME J. Heat Transf.* **2019**, *141*, 022401. [CrossRef]
36. Khan, A.; Shah, Z.; Islam, S.; Khan, S.; Khan, W.; Khan, Z.A. Darcy–Forchheimer flow of micropolar nanofluid between two plates in the rotating frame with non-uniform heat generation/absorption. *Adv. Mech. Eng.* **2018**, *10*, 1687814018808850. [CrossRef]
37. Shah, Z.; Bonyah, E.; Islam, S.; Khan, W.; Ishaq, M. Radiative MHD thin film flow of Williamson fluid over an unsteady permeable stretching. *Heliyon* **2018**, *4*, e00825. [CrossRef] [PubMed]
38. Jawad, M.; Shah, Z.; Islam, S.; Islam, S.; Bonyah, E.; Khan, Z.A. Darcy-Forchheimer flow of MHD nanofluid thin film flow with Joule dissipation and Navier's partial slip. *J. Phys. Commun.* **2018**. [CrossRef]

39. Khan, N.; Zuhra, S.; Shah, Z.; Bonyah, E.; Khan, W.; Islam, S. Slip flow of Eyring-Powell nanoliquid film containing graphene nanoparticles. *AIP Adv.* **2018**, *8*, 115302. [CrossRef]
40. Hammed, K.; Haneef, M.; Shah, Z.; Islam, I.; Khan, W.; Asif, S.M. The Combined Magneto hydrodynamic and electric field effect on an unsteady Maxwell nanofluid Flow over a Stretching Surface under the Influence of Variable Heat and Thermal Radiation. *Appl. Sci.* **2018**, *8*, 160. [CrossRef]
41. Dawar, A.; Shah, Z.; Khan, W.; Idrees, M.; Islam, S. Unsteady squeezing flow of MHD CNTS nanofluid in rotating channels with Entropy generation and viscous Dissipation. *Adv. Mech. Eng.* **2019**, *10*, 1–18. [CrossRef]
42. Khan, A.; Shah, Z.; Islam, S.; Dawar, A.; Bonyah, E.; Ullah, H.; Khan, Z.A. Darcy-Forchheimer flow of MHD CNTs nanofluid radiative thermal behaviour andconvective non uniform heat source/sink in the rotating frame with microstructureand inertial characteristics. *AIP Adv.* **2018**, *8*, 125024. [CrossRef]
43. Sheikholeslami, M.; Shah, Z.; Shafi, A.; Khan, I.; Itili, I. Uniform magnetic force impact on water based nanofluid thermal behavior in a porous enclosure with ellipse shaped obstacle. *Sci. Rep.* 2019. [CrossRef]
44. Feroz, N.; Shah, Z.; Islam, S.; Alzahrani, E.O.; Khan, W. Entropy Generation of Carbon Nanotubes Flow in a Rotating Channel with Hall and Ion-Slip Effect Using Effective Thermal Conductivity Model. *Entropy* **2019**, *21*, 52. [CrossRef]
45. Alharbi, S.O.; Dawar, A.; Shah, Z.; Khan, W.; Idrees, M.; Islam, S.; Khan, I. Entropy Generation in MHD Eyring–Powell Fluid Flow over an Unsteady Oscillatory Porous Stretching Surface under the Impact of Thermal Radiation and Heat Source/Sink. *Appl. Sci.* **2018**, *8*, 2588. [CrossRef]
46. Liao, S.J. On Homotopy Analysis Method for Nonlinear Problems. *Appl. Math. Comput.* **2004**, *147*, 499–513. [CrossRef]
47. Nasir, N.; Shah, Z.; Islam, S.; Bonyah, E.; Gul, T. Darcy Forchheimer nanofluid thin film flow of SWCNTs and heat transfer analysis over an unsteady stretching sheet. *AIP Adv.* **2019**, *9*, 015223. [CrossRef]
48. Tlili, I.; Khan, W.A.; Khan, I. Multiple slips effects on MHD SA-Al2O3 and SA-Cu non-Newtonian nanofluids flow over a stretching cylinder in porous medium with radiation and chemical reaction. *Results Phys.* **2018**, *8*, 213–221. [CrossRef]
49. Khan, N.S.; Shah, Z.; Islam, S.; Khan, I.; Alkanhal, T.A.; Tlili, I. Entropy Generation in MHD Mixed Convection Non-Newtonian Second-Grade Nanoliquid Thin Film Flow through a Porous Medium with Chemical Reaction and Stratification. *Entropy* **2019**, *21*, 139. [CrossRef]
50. Fiza, M.; Islam, S.; Ullah, H.; Shah, Z.; Chohan, F. An Asymptotic Method with Applications to Nonlinear Coupled Partial Differential Equations. *Punjab Univ. J. Math.* **2018**, *50*, 139–151.